Chemistry and Physics of Lipids 219 (2019) 15–22

Contents lists available at ScienceDirect

Chemistry and Physics of Lipids

journal homepage: www.elsevier.com/locate/chemphyslip

Lipidomic consequences of phospholipid synthesis defects in *Escherichia coli* revealed by HILIC-ion mobility-mass spectrometry

Kelly M. Hines, Libin Xu*

Department of Medicinal Chemistry, University of Washington School of Pharmacy, Seattle, WA, 98195, United States

ARTICLE INFO

Keywords:
Escherichia coli
Ion mobility
Mass spectrometry
Lipidomics
Phospholipids

ABSTRACT

Our understanding of phospholipid biosynthesis in Gram-positive and Gram-negative bacteria is derived from the prototypical Gram-negative organism *Escherichia coli*. The inner and outer membranes of *E. coli* are largely composed of phosphatidylethanolamine (PE), minor amounts of phosphatidylglycerol (PG) and cardiolipin (CL). We report here the utility of hydrophilic interaction liquid chromatography (HILIC) paired with ion mobility-mass spectrometry (IM-MS) for the comprehensive analysis of the *E. coli* lipidome. Using strains with chromosomal deletions in the PG and CL synthesis genes *pgsA* and *clsABC*, respectively, we show that defective phospholipid biosynthesis in *E. coli* results in fatty-acid specific changes in select lipid classes and the presence of the minor triacylated phospholipids, acylphosphatidyl glycerol (acylPG) and N-acylphosphatidylethanolamine (N-acylPE). Notably, acylPGs were accumulated in the *clsABC*-KO strain, but were absent in other mutant strains. The separation of 1-lyso and 2-lyso-phosphatidylethanolamines (lysoPEs) is demonstrated in both the HILIC and IM dimensions. Using our previously validated calibration method, collision cross section values of nearly 200 phospholipids found in *E. coli* were determined on a traveling wave IM-MS platform, including newly reported values for cardiolipins, positional isomers of lysoPEs, acylPGs and N-acylPEs.

1. Introduction

The Gram-negative organism *Escherichia coli* is one of the most widely studied bacterial species and much of what we currently know about the essential biosynthetic pathways in bacteria is derived from foundational studies performed in *E. coli*. Among those discoveries from *E. coli* is the phospholipid biosynthetic pathway that now serves as the template for phospholipid biosynthesis in both Gram-negative and Gram-positive species of bacteria (Kanfer and Kennedy, 1963, 1964). The delineation of the phospholipid synthesis pathway first began with an accounting of the phospholipid species present in *E. coli*. It was determined that roughly 70% of the *E. coli* lipidome at late log phase was phosphatidylethanolamine (PE), followed by phosphatidylglycerol (PG, 20%) and cardiolipin (CL, 5–10%) (Ames, 1968; Cronan, 1968; Kanemasa et al., 1967; Kanfer and Kennedy, 1963). These lipids all derive from the first phospholipid in the pathway, phosphatidic acid (PA, Fig. 1). After the conversion of PA to cytidine diphosphate diacylglycerol (CDP-DG), the phospholipid synthetic pathway forms two branches that lead to the synthesis of PEs or PGs and CLs.

The analytical tools used in those early studies were simple but highly informative. Cultures of *E. coli* were typically incubated in the presence of a radioactive isotope of phosphorus (i.e., ^{32}P in orthophosphate) for either a brief time in a technique called pulse labeling or fully isotopically labeled over several hours (Kanfer and Kennedy, 1963, 1964). The lipid extracts were hydrolyzed to generate phosphate esters, which were then separated by column and paper chromatography and detected by radioautography. Insight into the metabolism of phospholipids and their association with various growth phases was gained by incubating the pulse labeled cultures for different lengths of time in label-free conditions and monitoring the radioactivity (Cronan, 1968). Thin layer chromatography (TLC) was the preferred technique in assessing *E. coli* mutants with defective phospholipid synthesis as it

Abbreviations: acylPG, acylphosphatidylglycerol; N-acylPE or NAPE, N-acylphosphatidylethanolamine; CCS, collision cross section; CDP-DG, cytidine diphosphate diacylglycerol; CL, cardiolipin; DG, diacylglycerol; DTIM, drift tube ion mobility; FA, fatty acid; FFA, free fatty acid; HILIC, hydrophilic interaction liquid chromatography; IM, ion mobility; lysoPA, lysophosphatidic acid; lysoPE, lysophosphatidylethanolamine; MS, mass spectrometry; PA, phosphatidic acid; PE, phosphatidylethanolamine; PG, phosphatidylglycerol; PGP, phosphatidylglycerol phosphate; TLC, thin layer chromatography; TWIM, traveling wave ion mobility; XIC, extracted ion chromatogram

* Corresponding author at: Department of Medicinal Chemistry, University of Washington, Health Sciences Building, H-172, Box 357610, Seattle, WA, 98195, United States.

E-mail address: libinxu@uw.edu (L. Xu).

https://doi.org/10.1016/j.chemphyslip.2019.01.007
Received 10 November 2018; Received in revised form 16 January 2019; Accepted 16 January 2019
Available online 17 January 2019

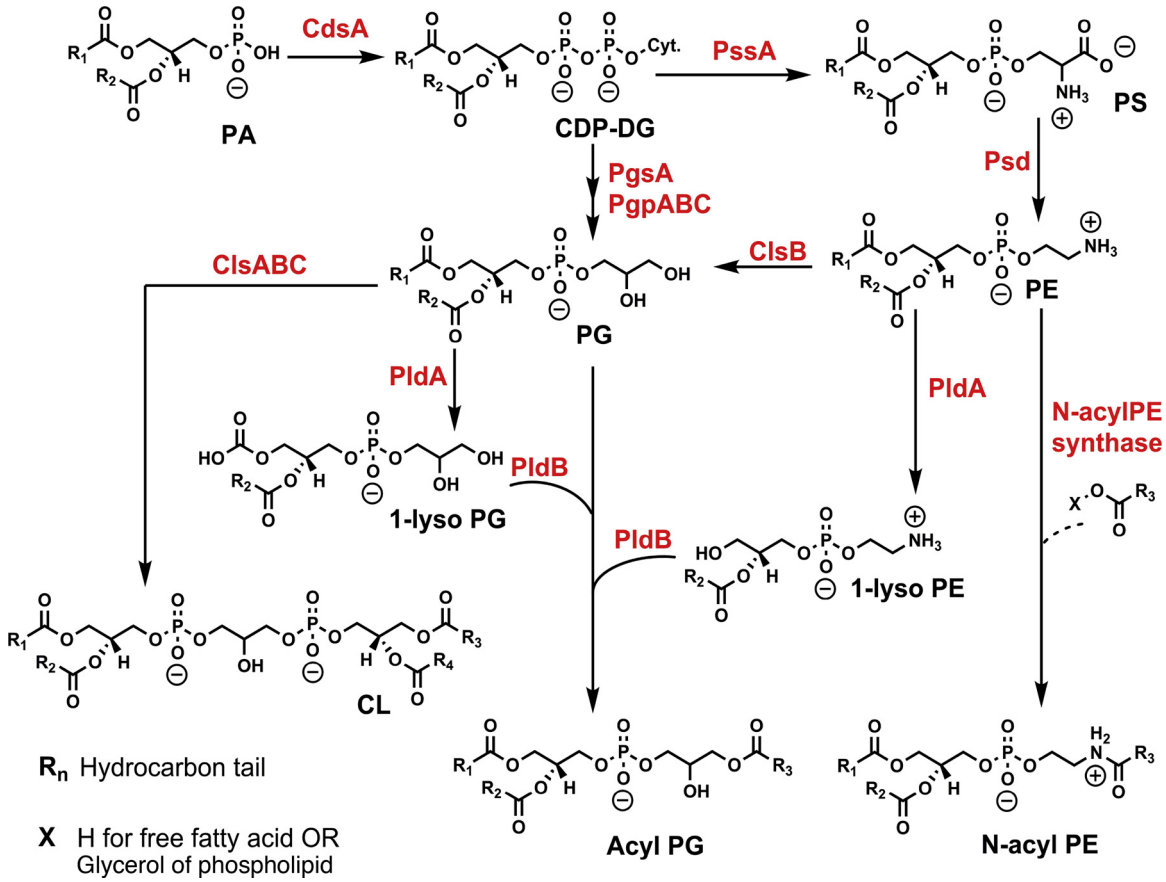

Fig. 1. Phospholipid biosynthesis pathway of *Escherichia coli*. A hypothetical N-acylPE synthase is shown acting on a substrate that is presumed to be a free fatty acid or the fatty acyl tail of a phospholipid.

provided a rapid read-out of the phospholipids present or absent in the lipid extracts of these strains (Shibuya et al., 1985). Spots identified as phospholipids by phosphorus-specific staining can be scraped from the plate for further analysis (Dittmer and Lester, 1964; Rouser et al., 1966). Additional experiments often included fatty acid analysis, in which the phospholipid was hydrolyzed to liberate the fatty acids and then fatty acid methyl esters were generated for gas chromatography-mass spectrometry analysis (Miller, 1982).

As analytical technologies improve, so does the amount of information that can be generated from a single analysis. However, there remain some challenges for the analysis and identification of lipids, the greatest among them being the large number of similar mass or isobaric lipids that naturally occur in any biological system. This high degree of overlap necessitates the use of multi-dimensional separation strategies to tease apart lipids with different backbones, headgroups, and fatty acids. In the field of eukaryotic lipidomics, both ultra-high-performance liquid chromatography (UHPLC) coupled to electrospray ionization (ESI)-high resolution mass spectrometry (HRMS) and shotgun lipidomics have been commonly used (Brown and Murphy, 2009; Ivanova et al., 2009; Han and Gross, 2005). Separation of lipids can be performed by normal-phase LC, in which lipids separate predominantly by headgroup polarity, or by reverse-phase LC to separate lipids on the basis of fatty acyl hydrophobicity. High-resolution mass spectrometers such as time-of-flight and orbitrap platforms can resolve nearly isobaric lipid species to varying degrees. However, the challenge of isobaric lipid species is one that typically requires a large investment of time into pre-analysis fractionation and longer or tandem chromatographic separations.

Ion mobility-mass spectrometry (IM-MS) is a hybrid technique that has gained acceptance in the lipidomics field over the past decade (Zheng et al., 2017). In an IM-MS experiment, gas-phase ions generated by soft ionization techniques, typically ESI, enter a cell that is pressurized with inert gas, commonly Helium or Nitrogen. A static electric field, as in drift tube IM (DTIM), or a dynamic electric field, as in traveling wave IM (TWIM), is applied across the length of the drift cell to push the ions forward. As ions transverse the drift cell under the influence of the electric field, they will also experience collisions with the inert gas. The number of ion-neutral collisions, and therefore the time required to traverse the drift cell (*i.e.*, drift time), is determined by the ion-neutral collision cross section (CCS, Ω) and related to the gas-phase conformation and size of the ion (Mason and McDaniel, 1988; Mason and Schamp, 1958). The result is that ions are separated first on the basis of structure-to-charge ratio in the IM dimension and then on the basis of mass-to-charge (m/z) ratio in the MS dimension.

While the chemical moieties that define the various subclasses of lipid species, such as the backbone, headgroup and fatty acyl composition, yield masses that may be too similar to be resolved by MS, they lead to distinct structures that are mostly resolvable in the IM dimension. Our group and several others have shown that IM-MS can resolve isobaric phospholipids arising from different headgroups, different connectivity of fatty acyls, and different locations of double bonds within the fatty acyls (Hines et al., 2017a; Kliman et al., 2011; Kyle et al., 2016; Paglia et al., 2015; Zhou et al., 2017). In positive ionization mode, some of the separation power of IM is mediated by different preferences for various cations among the lipid classes. However, the breadth of conformation space for lipids is relatively compacted in negative ionization mode (Hines et al., 2017a, 2016). This makes the identification of lipids on the basis of accurate mass and CCS more challenging in negative ionization mode than positive ionization mode. The difficulty with negative mode presents an issue for bacterial lipidomics studies as the membrane lipids of both Gram-positive and Gram-negative bacteria, such as PG, CL, and PE, tend to be weakly to strongly

anionic. The sensitivity of these lipid classes in ESI-MS analysis tends to be higher under negative ionization and slightly basic conditions (Han and Gross, 2005).

A further limitation to the use of CCS as an identifying parameter in lipidomics studies is the lack of reference CCS measurements (i.e., by DTIM instruments) for lipids. The major challenge to obtaining such reference CCS values is the lack of suitable standards for lipids and the time required to perform direct CCS measurements on many standards individually. The development of predictive algorithms for lipid CCS calculation using machine learning is a promising avenue to address this challenge (Zhou et al., 2017, 2018b). Furthermore, the Zhu lab has developed the first web-based platform, LipidIMMS Analyzer, for the comprehensive identification of lipids by accurate mass, retention times, predicted CCS value and *in silico* MS/MS fragmentation pattern (Zhou et al., 2018a).

We chose to pair hydrophilic interaction liquid chromatography (HILIC) with TWIM-MS as the separation of lipid classes based on headgroup polarity in the HILIC dimension is complementary to the subsequent IM-MS separation (Baker et al., 2014; Cifkova et al., 2012; Hines et al., 2017a, c). This approach has the benefits of simplifying lipid class determination, separating lipid classes that are prone to ionization suppression, and streamlining the interpretation of MS/MS data. The HILIC-IM-MS platform has been demonstrated for both mammalian and Gram-positive bacterial lipidomics analyses (Hines et al., 2017a, c). For bacterial lipids, the results of the HILIC separation are analogous to TLC or normal-phase chromatography while the IM-MS dimension provides details on individual lipid species that would have previously required several different experiments to achieve.

As previously demonstrated for Gram-positive bacteria, membrane lipid composition can vary widely between different species of bacteria (Hines et al., 2017c). In particular, the lipid profiles of Gram-positive and Gram-negative species differ dramatically: while Gram-negative membranes are composed predominantly of PEs, Gram-positive membranes lack PEs and are dominated by PGs. Here, we apply HILIC-IM-MS-based lipidomics to the analysis of *E. coli* strains with chromosomal deletions of the phospholipid biosynthesis genes *pgsA* and *clsABC* that result in defective synthesis of PGs and CLs (Li et al., 2016; Tan et al., 2012). Our results demonstrate the broad utility of the HILIC-IM-MS platform to assess anticipated class-level alterations in membrane phospholipids, as well as the detection of fatty acid-dependent changes in select lipid classes, and the detection and identification of minor triacylated phospholipids in *E. coli*. From these data, we report here the TWIM calibrated CCS ($^{TWIM}CCS_{N2}$) values for several classes and species of lipids for which CCS values have not previously been reported. Thus, this study also expands our previous collection of lipid CCS values with new measurements of *E. coli* phospholipids.

2. Materials and methods

2.1. Reagents

HPLC grade solvents (water, acetonitrile, chloroform, and methanol) and ammonium acetate (Optima LC/MS) were purchased from Thermo Fisher Scientific. Lyso-phosphatidylethanolamine (lysoPE) structural isomers containing oleic acid at the *sn-1* (Cat No. 846725) and *sn-2* (Cat No. 855725) positions were purchased from Avanti Polar Lipids (Alabaster, AL). Stock solutions of lipid standards were prepared at 1 mM in chloroform, from which a 5 μM solution in 2:1 acetonitrile/methanol was prepared for analysis. A mixture of representative bacteria lipids from standards and commercial extracts, and mixtures of phosphatidylcholines (PCs) and phosphatidylethanolamines (PEs) standards for CCS calibration were prepared as described previously (Hines et al., 2016, 2017c). Luria Broth (LB, low salt) and Tryptic Soy Agar for microbial growth were purchased from Sigma Life Sciences.

2.2. Bacteria strains

E. coli strains were purchased from the *E. coli* Genetic Stock Center (CGSC) at Yale University. The *E. coli* strains with chromosomal deletions of the cardiolipin synthase genes *clsA*, *clsB*, and *clsC* (*ΔclsABC*, CGSC No. 13593), phosphatidylglycerol synthase A (*ΔpgsA*, CGSC No. 13595), and deletions of *clsABC* and *pgsA* (*ΔclsABC + ΔpgsA*, CGSC No. 13596) were constructed by Brandon K. Tan et al. as described previously (Tan et al., 2012) and obtained from the CGSC. The location of these genes within the phospholipid biosynthetic pathway of *E. coli* is shown as Fig. 1. The *E. coli* K12 strain W3110 (CGSC No. 4474) was used as the wild-type reference strain in this work. All strains of *E. coli* were plated onto tryptic soy agar (TSA) and grown overnight at 37 °C. Colonies selected from these plates were used to prepare a 2.0 McFarland suspension (approx. 6.0×10^8 CFU/mL) from which 300 μL was used to inoculate 30 mL of sterile low-salt luria broth (LB). Cultures were incubated at 37 °C and shaken at 180 rpm overnight. Pellets were collected by centrifugation into pre-weighed 10 mL glass centrifuge tubes and dried in a SpeedVac concentrator (Thermo Scientific). Dried pellet weights ranged from 1 to 20 mg, with the *ΔpgsA* and *ΔclsABC + ΔpgsA* strains yielding substantially smaller pellets (1–3 mg) than the *ΔclsABC* strain and wild-type controls (10–20 mg) over the same growth period.

2.3. Sample preparation

Dried bacteria pellets were re-suspended in 1 mL of water and sonicated in an ice bath for 30 min. Lipid extraction was performed as described previously using a modified version of the Bligh and Dyer method (Bligh and Dyer, 1959). Briefly, 4 mL of chilled 2:1 methanol/chloroform was added to the aqueous pellet suspension and vortexed for 5 min, after which 1 mL of chilled chloroform and 1 mL of chilled water were added. Samples were vortexed for 1 min and centrifuged at 2000 × *g* for 10 min at 10 °C. The lower organic phase was collected into fresh 10 mL glass centrifuge tubes and dried in a SpeedVac concentrator. The dried extracts were reconstituted in 0.5 mL of 1:1 chloroform/methanol and stored at −80 °C in glass vials. For HILIC-IM-MS analysis, 5 μL of extract was transferred into glass vials and dried under a stream of nitrogen, after which 100 μL of 2:1 acetonitrile/methanol was added.

2.4. HILIC-IM-MS analysis

E. coli lipid extracts were separated by ultra-performance liquid chromatography (Waters Acquity I-Class FTN; Milford, MA) using a HILIC stationary phase (Phenomenex Kinetex, 2.1 × 100 mm, 1.7 μM) heated to 40 °C. The mobile phases for HILIC separation consisted of 95% acetonitrile/5% water with 5 mM ammonium acetate (HILIC A) and 50% acetonitrile/50% water with 5 mM ammonium acetate (HILIC B). As described previously, the 12 min gradient method started with 100% HILIC A and was gradually decreased to 70% HILIC A over 8 min using a flow rate of 0.5 mL/min before returning to 100% HILIC A. An injection volume of 5 μL was used for all samples.

The effluent from the HILIC separation was directed into the ESI source of a Synapt G2-Si HDMS (Waters) ion mobility-mass spectrometer that had been calibrated, as described previously (Hines et al., 2016), to generate accurate CCS values for lipids. As demonstrated in our previous work (Hines et al., 2016), calibration of CCS with the phospholipid standards allow us to obtain CCS values that are within 2% accuracy of those measured on a drift-tube instrument. In addition to the standard lipid CCS calibrants for calibrating singly charged lipid ions, a solution of poly-DL-alanine (25 μg/mL in 1:1 acetonitrile/water; Sigma Aldrich) was infused in positive and negative modes to generate a CCS calibration curve of doubly-charged ($z = 2$) poly-DL-alanine signals to be used for calibrating CCS values of doubly-charged cardiolipin ions. Conditions for the ESI source were as follows: capillary

voltage, -2.0 kV (neg mode) and + 2.5 kV (pos mode); sampling cone, 40 V; extraction cone, 80 V; source temperature, 150 °C; desolvation temperature, 350 °C; cone gas, 100 L/hr; desolvation gas, 1000 L/hr. TWIM separation was performed in Nitrogen gas with a traveling wave velocity of 500 m/s and height of 40 V (refer to Supplementary Materials for additional IM parameters). Data was acquired for the range of *m/z* 50–1200 with a 1 s scan time using an untargeted MS/MS method (MS^E) in which the collision energy in the Transfer region (after ion mobility separation) of the instrument was ramped over 35–45 eV. Leucine enkephalin lockspray signal was acquired throughout the run for correction of drift in *m/z* and drift time over time.

2.5. Data analysis

Post-acquisition data alignment, peak detection, and normalization to dry pellet weight was performed in Progenesis QI (Nonlinear Dynamics). A pooled quality control (QC) sample was used as the reference alignment. Peak picking in the chromatographic dimension was performed with the highest sensitivity over the range of 0.4 to 9.0 min. Student's t-tests for two sample groups were performed using a two-tailed distribution with equal variance. Lipid identifications were made from an in-house database of bacterial lipids that was expanded upon from the original LipidPioneer (Ulmer et al., 2017) database and using a mass accuracy threshold of 15 ppm. Calibrated CCS values of mono- and di-acyl phospholipids were obtained using the DriftScope v2.8 (Waters) Apex3D algorithm with lockspray mass and drift time correction. For tri-acyl phospholipids, manually extracted and Gaussian-fitted drift time profiles were used to obtain calibrated CCS values. CCS values for doubly-charged cardiolipins in positive and negative modes were calibrated manually using Apex3D-detected drift times and previously reported $^{DTIM}CCS_{N2}$ values for $z = 2$ poly-DL-alanine signals. Parameters for all CCS calibration curves may be found in the Supplementary Materials. Reported standard deviations for calibrated CCS values are from intra-day triplicate measurements.

3. Results

3.1. Detailed lipidomic changes resulting from deletion of clsABC and/or pgsA in E. coli

All major classes of *E. coli* phospholipids were observed using the HILIC-IM-MS method. Representative IM-extracted ion chromatograms (IM-XICs), which contain only signals with lipid-like drift times, are shown in Fig. 2 for each *E. coli* strain. The wild-type strain, W3110, demonstrates that the major lipid species in *E. coli* membranes are phosphatidylethanolamines (PEs, 5.5 min), followed by phosphatidylglycerols (PGs, 2–3 min), lyso-phosphatidylethanolamines (lysoPEs, 6.5–7 min), and cardiolipins (CLs, 4.5–5.5 min). Free fatty acids were present at 0.77 min in negative ionization mode (Table S6), which appears to be consistent with the collective fatty acid composition of CLs obtained from negative mode MS^E fragmentation, in which the intensities of fatty acid anions decrease in the order of 16:0, 16:1, 17:1, 18:1, 14:0, 15:0, and 19:1 (Figure S1).

In addition to these major phospholipids, the HILIC-IM-MS method also detected the presence of several minor species of *E. coli* phospholipids. Two chromatographic peaks at 0.8 and 1.6 min contained signals with lipid-like drift times and *m/z* values in the range of 850 to 1050 Da. Untargeted fragmentation data was acquired throughout the HILIC-IM-MS run, with the collision-induced dissociation occurring post-ion mobility separation. This method provides mobility-organized fragmentation spectra such that the fragment ions align in drift time with their precursors, and thus, fragmentation spectra for different precursors can be specifically isolated on the drift time scale, effectively eliminating interference from non-aligned ions (see Figure S2 for an example). Examination of the untargeted MS/MS data at 0.8 min in positive ionization mode revealed two clusters of fragment ions

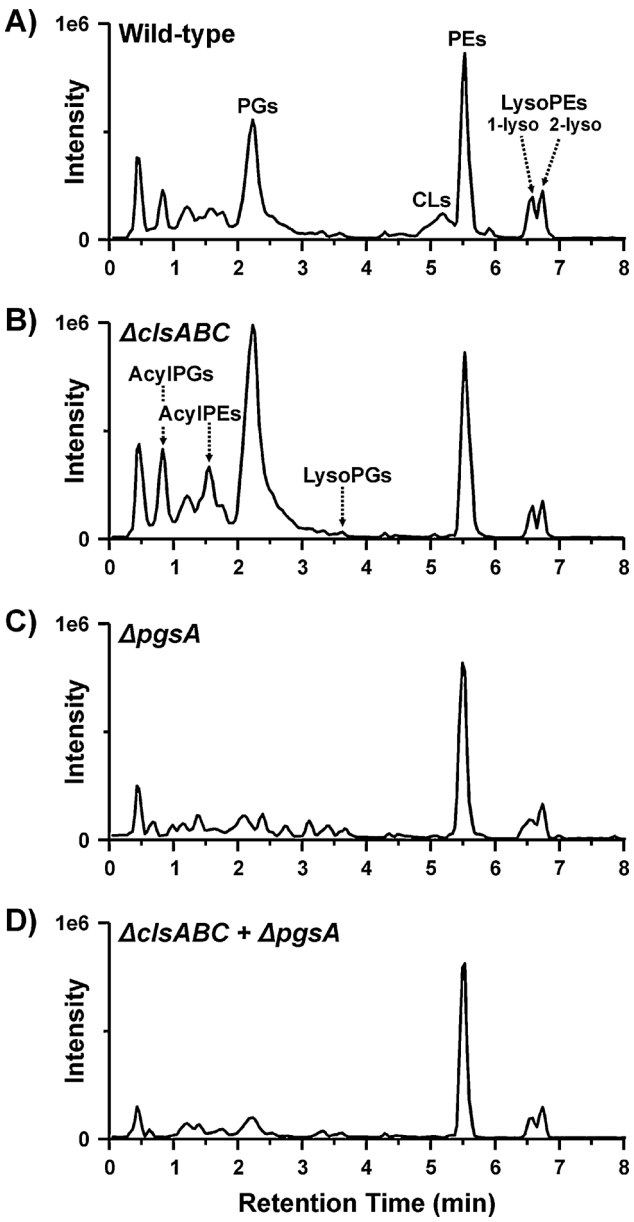

Fig. 2. Ion mobility extracted ion chromatograms of *E. coli* strains from positive ionization mode.

centered around 445.27 and 563.55 Da (Figure S3). These fragment masses corresponded to sodium adducts of lysophosphatidic acids (lysoPAs) and protonated diacylglycerols (DGs) with a water loss with the major species being 17:1 and 33:1, respectively. Based on these data and accurate mass, it was determined that the species at 0.8 min corresponded to acylated phosphatidylglycerol (acylPG). As expected, acylPGs were only accumulated in the *ΔclsABC* strain, but were absent in the two other mutant strains.

The unknown at 1.6 min generated more complex untargeted MS/MS spectra with clusters of fragment ions centers around 683.45, 563.50, 402.24, and 282.28 Da in positive ionization mode (Figure S4). As with the acylPGs, the fragments center around *m/z* 563.50 corresponded to DG $[M+H\text{-}H_2O]^+$ ions with the major species being 33:1. The remaining masses were searched against lipid databases. The fragments centered around *m/z* 683.45 corresponded to $[M+Na]^+$ ions of PAs. The fragments with *m/z* 282.28 and 402.24 corresponded to oleamide and N-palmitoyl-phosphoethanolamine, respectively. From these data it was determined that the unknown lipid species at 1.6 min was N-acylphosphatidylethanolamine (N-acylPE or NAPE).

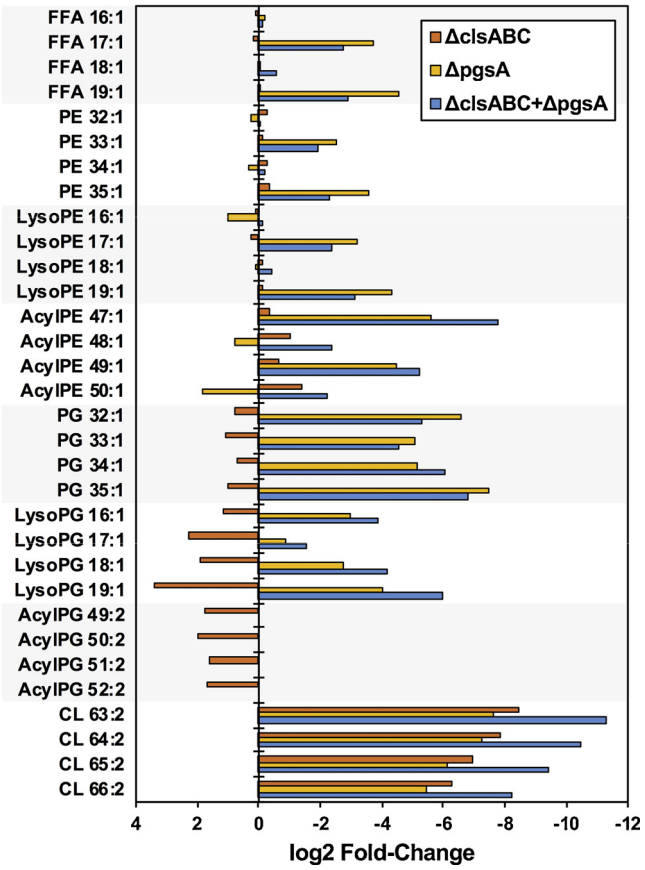

Fig. 3. Lipid changes observed in *E. coli* strains with defective phospholipid biosynthesis displayed as log2 fold-change relative to wild-type *E. coli*. The *p*-values from Student's *t*-test for these lipidomic changes can be found in Tables S1–S8 in the Supplementary Materials.

The chromosomal deletions of *clsABC* and *pgsA* had substantially different effects on the *E. coli* lipidome. The Δ*clsABC* strain (Fig. 2B) had diminished levels of CLs and higher levels of PGs, lysoPGs (3.6 min, Table S5), and acylPGs, relative to the WT strain (Fig. 3). Deletions of *pgsA*, alone or in combination with deletion of *clsABC*, had the most significant effect on the *E. coli* lipid profiles (Fig. 2C and D). PGs and other phospholipid species derived from PGs (Fig. 1), including cardiolipins, lysoPGs, and acylPGs, were decreased or absent from the *ΔpgsA* and *ΔclsABC + ΔpgsA* strains (Fig. 3). PE-derived lipids and free fatty acids (FFAs) were also affected by the knockout of *pgsA*. PEs with fatty acid compositions of 33:1 and 35:1 were decreased in the *ΔpgsA* and *ΔclsABC + ΔpgsA* strains, whereas the other major PE species were unaffected (Fig. 3). LysoPEs 17:1 and 19:1 and the corresponding FFAs were similarly decreased. Minor amounts of N-acyl-PEs were also observed in all strains with several species decreased in the absence of *pgsA* (Fig. 3). However, there was no statistical significance between knockout and wild-type strains (Table S3).

3.2. Resolution of E. coli lipid classes and isomers by HILIC and IM-MS

As shown in Fig. 2, the HILIC method achieved separation of lysoPE positional isomers arising from the attachment of the acyl chain to the *sn-1* (referred to as 1-acyl-2-lyso-PE or 2-lysoPE) or *sn-2* (referred to as 1-lyso-2-acyl-PE or 1-lysoPE) position of the glycerol backbone. We did not observe this phenomenon in our previous work with HILIC separation of mammalian lipid extracts in which lysoPEs were also observed. However, we have confirmed with analytical standards of lysoPE 18:1 that lysoPEs with the acyl chain at the *sn-2* position elute prior to the lysoPE with the acyl chain at *sn-1* (Figure S5). We observed

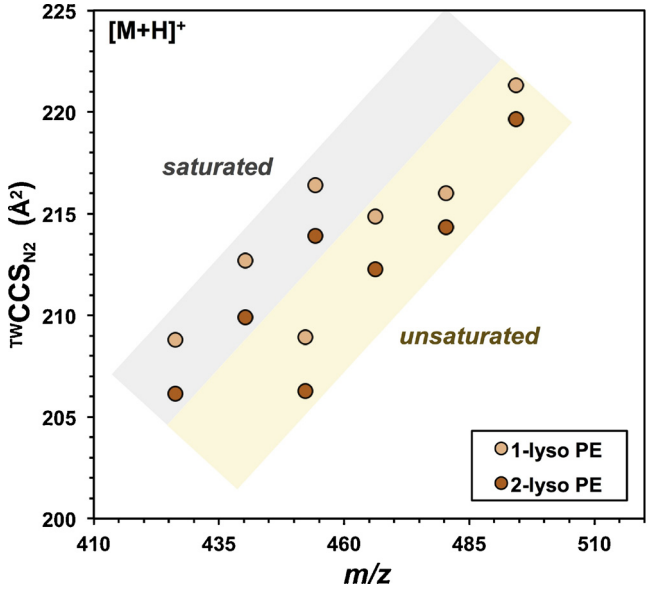

Fig. 4. Separation of 1-acyl-2-lyso and 1-lyso-2-acyl PEs in wild-type *E. coli* by IM-MS in positive ionization mode.

a similar bimodal chromatographic peak shape for lyso-phosphatidylglycerols (lysoPGs) in WT and *ΔclsABC* lipid extracts (Figure S6). Although the separation order is likely the same as that of lysoPEs, we cannot confirm such conclusion due to lack of standards.

In addition to separation in the chromatographic dimension, we observed resolution of 1- and 2-lysoPEs in the IM dimension, but only for the protonated species in positive ionization mode (Fig. 4). The 1-lysoPEs have CCS values that are 0.7 to 1.3% percent larger than the CCS values of 2-lysoPEs with the same fatty acid composition. This trend holds for both fully saturated and unsaturated lysoPEs, but the magnitude of the difference decreased with increasing fatty acid tail length. CCS values of sodium adducts of 2- and 1-lysoPEs differed by less than 0.5%. From the standards of 2- and 1-lysoPE 18:1 (Figure S7), it was determined that the protonated structural isomers differed in CCS by 1.06% and the sodium adducts differed by 0.68% with the 2-acyl-1-lyso species having the larger CCS value (Table S10). The calibrated CCS values of the 2- and 1-lysoPE 18:1 standards are in good agreement with the values determined from the *E. coli* lipid extracts, differing by only 0.23% and 0.52%, respectively, for protonated adducts in positive mode.

A complete picture of the conformation landscape of *E. coli* phospholipids is shown in Fig. 5A and B. We have obtained CCS values for phospholipids containing one (lysoPGs and lysoPEs), two (PAs, PE, PGs), three (acylPGs and acylPEs), and four (CLs) fatty acyl chains, many of which are reported in both negative (Fig. 5A) and positive (Fig. 5B) modes. In negative mode, the CCS values of phospholipids scale nearly linearly with the addition of one more fatty acid. Monoacyl and di-acyl phospholipids, observed as $[M-H]^-$ ions, are not resolved in the IM dimension in negative mode. However, there is a clear separation between acylPE and acylPGs with the acylPEs being the larger of the two. In addition to four fatty acid tails, cardiolipins also have an additional phosphoglycerol group that results in a larger increase in mass from tri- to tetra-acyl than is observed for di- to tri-acyl phospholipids. The additional phosphoglycerol group can accommodate a second proton loss in negative ionization mode to form doubly-charged ions, represented as $[M\text{-}2\,H]^{2-}$ and plotted with their accurate masses, instead of *m/z*, in Fig. 5A.

We also observed cardiolipins in the positive mode data in the form of doubly-charged ions arising from adduction with two potassium ions, i.e. $[M+2K]^{2+}$. The formation of $[M+2K]^{2+}$ ions for cardiolipins was confirmed with commercial extracts enriched for cardiolipins that we

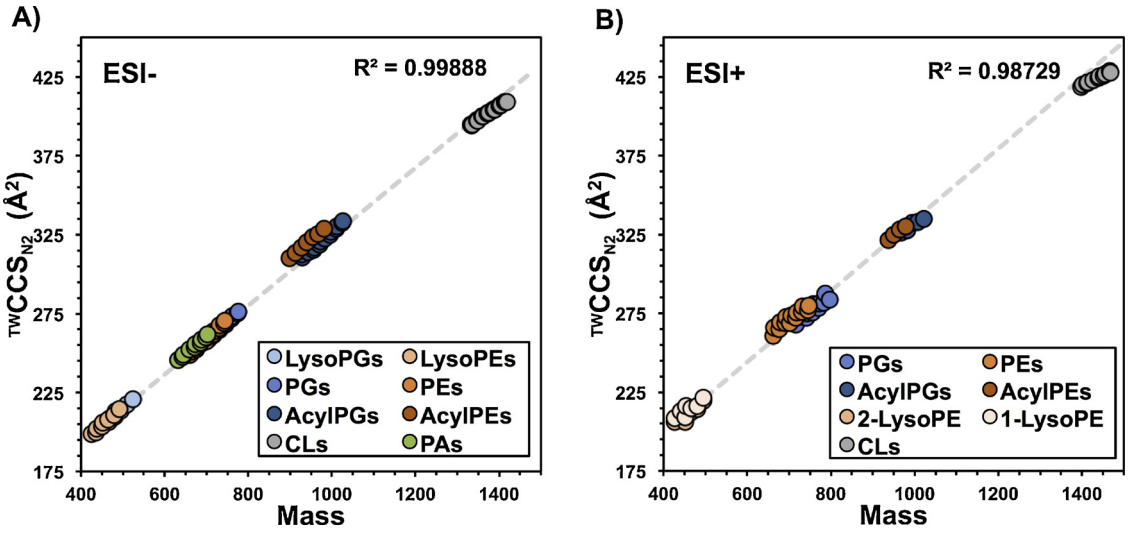

Fig. 5. IM-MS plots of the $^{TWIM}CCS_{N2}$ values of phospholipids found in *E. coli* in A) negative ionization mode and B) positive ionization mode with linear trendlines fit to monoacyl and diacyl phospholipids.

have previously characterized. Given the presence of two K^+ atoms, the CCS values of cardiolipins in positive mode lie below the general trendline of *E. coli* phospholipids. The separation of acylPEs and acylPGs by CCS is reduced in positive mode, where acylPEs appear as protonated ions and acylPGs appear as sodium adducted ions. In contrast, there appears to be greater separation of PEs and PGs in positive mode than seen in negative mode, consistent with our previous observation (Hines et al., 2017a). Similar to their tri-acylated counterparts, PEs form predominantly protonated ions whereas PGs ionize intact in positive mode as sodium adducted ions. LysoPGs and PAs were not observed as intact parent ions in positive ionization mode.

4. Discussion

The lipid synthetic pathway of *E. coli* consists of a branching point at the formation of CDP-DG from PA (Fig. 1). From CDP-DG, the synthesis of PE occurs through the formation of phosphatidylserines (PS) via phosphatidylserine synthase A (PssA), followed by decarboxylation of PS by phosphatidylserine decarboxylase (Psd) to generate PE. In the other direction, synthesis of PG and CL proceeds from CDP-DG through the synthesis of phosphatidylglycerol phosphate (PGP) by PgsA and dephosphorylation of PGP by PgpABC to yield PG. The PG branch of the *E. coli* lipid synthetic pathway then continues to the formation of cardiolipins from PGs by the cardiolipin synthases (ClsABC).

In this study, we characterized the lipidomes of wild type and three mutant strains of *E. coli*, generated by Tan et al., that lack *pgsA*, *clsABC*, or both *pgsA* and *clsABC* (Tan et al., 2012). Our analysis of wild-type *E. coli* by HILIC-IM-MS revealed the expected distribution of phospholipids, with PEs being the most abundant, followed by PGs and CLs. We also noted a significant amount of lysoPEs, low levels of acylPGs and N-acylPEs, and trace amounts of lysoPGs in the wild-type strain and varied levels of these lipids in the mutant strains. These species were not reported in previous lipidomics analyses of these strains by Tan et al., perhaps due to lower sensitivity of their methods (TLC and normal phase LC–MS).

While changes in the total abundance of each of these species could be determined from other methodologies, such as TLC, the observation of specific changes within individual lipid classes would likely be missed. Using the HILIC-IM-MS method for bacterial lipidomics, we were able to observe both the dramatic changes in the overall abundance of major *E. coli* lipids as well as the more nuanced changes to the distribution of individual lipid species within those classes in lipid synthesis mutant strains. For example, the reduction in select PE and lysoPEs species in the *ΔpgsA* and *ΔclsABC+ΔpgsA* strains is not discernable from the IM-XICs (Fig. 2) and would likely not be discernable by TLC either. Thus, our analysis revealed greater detail on the *E. coli* lipidome in general and on lipidomic consequences of deletions in *pgsA* and/or *clsABC*.

The highest levels of acylPGs were observed in the *ΔclsABC* mutant strain, whereas N-acylPEs were at the highest levels in wild-type *E. coli* with the exceptions of elevated levels of N-acylPEs 48:1 and 50:1 in the *ΔpgsA* mutant strain. We observed that the major acylPGs tended to have a total of two degrees of unsaturation in their fatty acyl tails, whereas the major PGs contained just one degree of unsaturation in their fatty acyl tails. This is consistent with early reports on the synthesis of acylPGs in *E. coli* where it was demonstrated that a fatty acid from the *sn-2* acyl tail of lysoPE or lysoPG was transferred onto the glycerol headgroup of a PG to form acylPG (Kobayashi et al., 1980; Nishijima et al., 1978). The *sn-2* position of the major *E. coli* PEs (and PGs as well) tends to contain a fatty acid with one degree of unsaturation (double bond or cyclopropyl) (Oursel et al., 2007), thus explaining the presence of an additional degree of unsaturation in acylPGs.

The exact mechanism of N-acylPE synthesis in *E. coli* is not currently known and N-acylPE synthesis occurs differently in plants and mammals. As such, we have shown in Fig. 1 a hypothetical NAPE synthase using a generic acyl group as the substrate for N-acylPE synthesis. The source of the PE headgroup acyl is either derived from another phospholipid as in mammals (Schmid et al., 1996) and similar to acylPG synthesis, or from a free fatty acid as in plants (Chapman, 2000). However, unlike acylPGs, we observed that N-acylPEs contain the same degree of unsaturation as that of their PE precursors. The total carbon number of the fatty acyl tails of the major N-acylPEs was also lower than those of the acylPGs by two carbons. Given that the major species of PEs and PGs shared the same number of total carbons in their fatty acyl tails (32–35 carbons), the finding on the differences in the degree of unsaturation and total number of carbons between acylPGs and N-acylPEs suggests that the enzyme performing N-acylation of PEs requires shorter and fully saturated fatty acids than PldB.

PEs are zwitterionic non-bilayer lipids, but N-acylation of PEs yields an anionic non-bilayer lipid (Dowhan, 2013). PGs, on the other hand, are anionic bilayer lipids and acylation does not affect the anionic properties of the PGs but does result in the transformation of a bilayer lipid into a non-bilayer lipid. The major anionic non-bilayer lipids in *E. coli* are typically CLs and PAs, which are localized to regions of the cell with a high degree of negative curvature such as the cell poles and the

cell division site (Dowhan, 2013; Mileykovskaya and Dowhan, 2000, 2005). The absence of CLs sensitizes cells to low osmolarity (Shibuya et al., 1985) and can disrupt the organization of membrane proteins involved in DNA replication initiation and cell division (Mileykovskaya and Dowhan, 2005). The headgroup acylated phospholipids can act to stabilize the membrane curvature during cell division and were proposed to segregate to the cell poles and cell division site in a manner similar to CLs and PAs (Dowhan, 2013; Huang et al., 2006; Mileykovskaya et al., 2009). Thus, the presence of acylPG and N-acylPE may mitigate some of the deleterious effects of the *ΔclsABC*, as evidenced by the negligible differences in the pellet sizes from overnight cultures of wild-type and *ΔclsABC* strains (13.1 ± 3.4 mg vs 17.0 ± 5.8 mg, respectively; $p = 0.46$).

Although synthesis of acylPGs requires 2-acyl lysoPEs or lysoPGs, we did not observe any changes to the total levels of lysoPEs or the ratio of 1-lyso to 2-lyso phospholipids in the *ΔclsABC* mutant strain (Fig. 2A and B). However, lysoPGs were increased in the *ΔclsABC* mutant strain and lysoPE species containing 17:1 and 19:1 fatty acids were decreased in both the *ΔpgsA* and *ΔpgsA* + *ΔclsABC* mutant strains. In these two strains, free fatty acids 17:1 and 19:1 were decreased as well as PE species presumed to contain 17:1 and 19:1 fatty acids such as PE 33:1 (17:1 and 16:0) and PE 35:1 (19:1 and 16:0) (see Figure S8 for fatty acid fragments from MS^E of PEs in negative mode). Fatty acids 17:1 and 19:1 are presumed to be cyclopropyl fatty acids formed from the addition of a methylene group across the double bonds of *cis*-16:1 and *cis*-18:1 fatty acids by cyclopropane fatty acid synthase. This reaction occurs predominantly to inner membrane unsaturated fatty acids as *E. coli* enters the stationary phase (Wang and Cronan, 1994). Cyclopropane fatty acids protect against acid sensitivity and other environmental stresses (Chang and Cronan, 1999). Compared to fatty acids with double bonds, cyclopropane fatty acids stabilize membranes and increase fluidity (Poger and Mark, 2015). In the context of our findings, the decreased levels of PEs and lysoPEs with cyclopropane fatty acids in the *ΔpgsA* and *ΔclsABC* + *ΔpgsA* mutant strains suggests a shift towards more rigid but less ordered membranes in the absence of PGs and CLs.

As shown in Fig. 1, ClsB has a secondary function in *E. coli*, which is the synthesis of PGs from PEs in the absence of PgsA and with a supply of free glycerol moieties. This function of ClsB was first demonstrated by Li and co-workers after their observation of PGs and CLs in this same *ΔpgsA* strain (Li et al., 2016). By complementation with plasmids containing individual cardiolipin synthases, Li et al. determined that PGs and CLs were present only in the *ΔpgsA* + *ΔclsABC* mutant strain that was complemented with ClsB when 0.4% glycerol was added. However, we did not observe trace amounts of PGs and CLs in the *ΔpgsA* mutant, likely because we did not supplement our cultures with the required 0.4% glycerol.

Resolution of positional isomers of lysoPEs. The separation of lysoPEs based on the fatty acyl position is a new observation with the HILIC-IM-MS method. Our previous observation of lysoPEs with the HILIC-IM-MS method was in the context of mammalian systems where the 1-acyl lysoPEs is the major species (Hines et al., 2017a; Okudaira et al., 2014). From our analysis of lysoPEs standards, we have been able to resolve the 1-oleic and 2-oleic positional isomers in the chromatographic dimension and in the ion mobility dimension. In the HILIC separation, the 2-acyl-1-lyso isomer elutes prior to the 1-acyl-2-lyso isomer. This suggests that the lysoPEs with the fatty acyl on the *sn-2* position of the glycerol backbone are less hydrophilic (or polar) than their *sn-1* counterparts. We observed a significant amount of 1-oleoyl lysoPEs in the commercial standard of 2-oleoyl lysoPEs. This is a known rearrangement observed in synthetic lysophospholipids that arises from the migration of the fatty acyl from the *sn-2* to the *sn-1* position (Pluckthun and Dennis, 1982). With the ability of the HILIC method to separate 1- and 2-lysoPEs, we have been able to measure with high confidence the CCS values of 1-oleoyl lysoPEs and 2-oleoyl lysoPEs for the first time to our knowledge. The 2-acyl-1-lyso isomer has a consistently larger CCS value than the 1-acyl-2-lyso isomer with the same fatty acid by 1% CCS on average in both commercial and natural sources. This degree of separation is well outside the intra- and inter-day variability we routinely observe in our own measurements (Hines et al., 2017a, 2016; Hines et al., 2017b) and those reported for DTIM measurements (Stow et al., 2017; Gabelica et al., 2018).

CCS values of acylphospholipids and cardiolipins. We also report here, for the first time to our knowledge, the CCS values of triacylated phospholipids and cardiolipins in positive and negative ionization modes (Fig. 5). Our lipid CCS calibrants are based on PE and PC species that ionize in negative and positive modes, respectively, as singly-charged ions (Hines et al., 2016), which make them good calibrants for the singly charged monoacyl, diacyl, and triacyl lipid species in this study. Cardiolipins, however, ionize as double charged species in both negative and positive modes. While their *m/z* values fall within the range of *m/z* covered by our lipid CCS calibrants, their drift times are significantly lower than those of the PEs and PCs because the repulsive force of the traveling wave increases with the charge state of the ion. Thus, a different CCS calibration regime was utilized to generate CCS values for CLs. Bush and co-workers have shown that there is a large difference in reciprocal mobilities in N_2 between ions of singly charged and doubly or multiply charged when correlated with matching values in He (Bush et al., 2012). This observation results from larger polarization of N_2 by ions with larger charge density. Furthermore, general compaction of the ion mobility experiment as charge increases leads to shorter drift times, reducing the breadth of conformation space. Based on these reasonings, the use of charge-matched CCS calibrants is more important than the use of structure-matched calibrants for the determination of CCS values of multiply charged ions. Thus, we used the doubly-charged series of poly-DL-alanine ions as CCS calibrants for the determination of CL CCS values in positive (Bush et al., 2012) and negative (Allen et al., 2016) ionization modes. We suspect that, given the formation of $[M+2K]^{2+}$ ions, the calibrated CCS values of CLs in positive mode may have a larger error due to the difference in the atomic radii of K and H atoms. However, drift tube measurements of CLs have not been reported for neither negative mode nor positive mode ions and therefore it is not yet possible to determine the accuracy of our calibrated CCS values.

5. Conclusions

As the tools for the study of lipidomics improve, we are able to define the composition of biological systems in greater detail and to observe changes at the level of individual lipid species rather than lipid class. We have shown here that the HILIC-IM-MS method for bacterial lipidomics is able to capture the major remodeling of *E. coli* membrane lipids due to the chromosomal deletions of *pgsA* and *clsABC*, as well as fatty acid-specific changes to PE-derived *E. coli* lipids, and the presence and alterations of the minor triacylated phospholipids, acylPG and N-acylPE. The HILIC-IM-MS method offers the added advantage of resolving the positional isomers of *sn-1* and *sn-2* lysoPE, which serve distinct roles in the lipid biosynthetic pathway of *E. coli*, in both the chromatographic and ion mobility dimensions. Collectively, we determined the CCS values of nearly 200 lipid species, including those of cardiolipins, positional isomers of lysoPEs, acylPGs, and N-acylPEs that are reported here for the first time. The HILIC-IM-MS platform provides unparalleled information spanning from lipid class identification to the stereospecificity lysophospholipids. The ability to define the lipidome of prokaryotic systems to such depth will provide new insight into the roles of individual lipid species in the larger pathway of lipid biosynthesis.

Acknowledgements

This study was supported by the University of Washington (UW) School of Pharmacy Faculty Innovation Fund, UW Royalty Research Fund (A128444), National Institutes of Health (R01AI136979), and the

startup fund to LX from the Department of Medicinal Chemistry in the School of Pharmacy at the UW. We would like to thank the technical assistance of Prof. Brian Werth in the Department of Pharmacy at the UW on culturing *E. coli*.

Appendix A. Supplementary data

Supplementary data associated with this article can be found, in the online version, at https://doi.org/10.1016/j.chemphyslip.2019.01.007.

References

Allen, S.J., Giles, K., Gilbert, T., Bush, M.F., 2016. Ion mobility mass spectrometry of peptide, protein, and protein complex ions using a radio-frequency confining drift cell. Analyst 141, 884–891.

Ames, G.F., 1968. Lipids of Salmonella typhimurium and Escherichia coli – structure and metabolism. J. Bacteriol. 95, 833–843.

Baker, P.R.S., Armando, A.M., Campbell, J.L., Quehenberger, O., Dennis, E.A., 2014. Three-dimensional enhanced lipidomics analysis combining UPLC, differential ion mobility spectrometry, and mass spectrometric separation strategies. J. Lipid Res. 55, 2432–2442.

Bligh, E.G., Dyer, W.J., 1959. A rapid method of total lipid extraction and purification. Can. J. Biochem. Physiol. 37, 911–917.

Brown, H.A., Murphy, R.C., 2009. Working towards an exegesis for lipids in biology. Nat. Chem. Biol. 5, 602–606.

Bush, M.F., Campuzano, I.D.G., Robinson, C.V., 2012. Ion mobility mass spectrometry of peptide ions: effects of drift gas and calibration strategies. Anal. Chem. 84, 7124–7130.

Chang, Y.Y., Cronan, J.E., 1999. Membrane cyclopropane fatty acid content is a major factor in acid resistance of Escherichia coli. Mol. Microbiol. 33, 249–259.

Chapman, K.D., 2000. Emerging physiological roles for N-acylphosphatidylethanolamine metabolism in plants: signal transduction and membrane protection. Chem. Phys. Lipids 108, 221–229.

Cifkova, E., Holcapek, M., Lisa, M., Ovcacikova, M., Lycka, A., Lynen, F., Sandra, P., 2012. Nontargeted quantitation of lipid classes using hydrophilic interaction liquid chromatography-electrospray ionization mass spectrometry with single internal standard and response factor approach. Anal. Chem. 84, 10064–10070.

Cronan, J.E., 1968. Phospholipid alterations during growth of Escherichia coli. J. Bacteriol. 95, 2054–2061.

Dittmer, J.C., Lester, R.L., 1964. A simple, specific spray for the detection of phospholipids on thin-layer chromatograms. J. Lipid Res. 5, 126–127.

Dowhan, W., 2013. A retrospective: use of Escherichia coli as a vehicle to study phospholipid synthesis and function. Biochim. Et Biophys. Acta-Mol. Cell Biol. Lipids 1831, 471–494.

Han, X., Gross, R.W., 2005. Shotgun lipidomics: electrospray ionization mass spectrometric analysis and quantitation of cellular lipidomes directly from crude extracts of biological samples. Mass Spectrom. Rev. 24, 367–412.

Hines, K.M., May, J.C., McLean, J.A., Xu, L., 2016. Evaluation of collision cross section calibrants for structural analysis of lipids by traveling wave ion mobility-mass spectrometry. Anal. Chem. 88, 7329–7336.

Hines, K.M., Herron, J., Xu, L., 2017a. Assessment of altered lipid homeostasis by HILIC-ion mobility-mass spectrometry-based lipidomics. J. Lipid Res. 58, 809–819.

Hines, K.M., Ross, D.H., Davidson, K.L., Bush, M.F., Xu, L., 2017b. Large-scale structural characterization of drug and drug-like compounds by high-throughput ion mobility-mass spectrometry. Anal. Chem. 89, 9023–9030.

Hines, K.M., Waalkes, A., Penewit, K., Holmes, E.A., Salipante, S.J., Werth, B.J., Xu, L., 2017c. Characterization of the mechanisms of daptomycin resistance among gram-positive bacterial pathogens by multidimensional lipidomics. mSphere 2, e00492–00417.

Huang, K.C., Mukhopadhyay, R., Wingreen, N.S., 2006. A curvature-mediated mechanism for localization of lipids to bacterial poles. PLoS Comput. Biol. 2, e151.

Ivanova, P.T., Milne, S.B., Myers, D.S., Brown, H.A., 2009. Lipidomics: a mass spectrometry based systems level analysis of cellular lipids. Curr. Opin. Chem. Biol. 13, 526–531.

Kanemasa, Y., Akamatsu, Y., Nojima, S., 1967. Composition and turnover of the phospholipids in Escherichia coli. Biochim. Biophys. Acta 144, 382–390.

Kanfer, J., Kennedy, E.P., 1963. Metabolism and function of bacterial lipids. I. Metabolism of phospholipids in Escherichia coli B. J. Biol. Chem. 238, 2919–2922.

Kanfer, J., Kennedy, E.P., 1964. Metabolism and function of bacterial lipids. Ii. Biosynthesis of phospholipids in Escherichia coli. J. Biol. Chem. 239, 1720–1726.

Kliman, M., May, J.C., McLean, J.A., 2011. Lipid analysis and lipidomics by structurally selective ion mobility-mass spectrometry. Biochim. Et Biophys. Acta-Mol. Cell Biol. Lipids 1811, 935–945.

Kobayashi, T., Nishijima, M., Tamori, Y., Nojima, S., Seyama, Y., Yamakawa, T., 1980. Acyl phosphatidylglycerol of Escherichia-coli. Biochim. Biophys. Acta 620, 356–363.

Kyle, J.E., Zhang, X., Weitz, K.K., Monroe, M.E., Ibrahim, Y.M., Moore, R.J., Cha, J., Sun, X., Lovelace, E.S., Wagoner, J., Polyak, S.J., Metz, T.O., Dey, S.K., Smith, R.D., Burnum-Johnson, K.E., Baker, E.S., 2016. Uncovering biologically significant lipid isomers with liquid chromatography, ion mobility spectrometry and mass spectrometry. Analyst 141, 1649–1659.

Li, C., Tan, B.K., Zhao, J., Guan, Z., 2016. In vivo and in vitro synthesis of phosphatidylglycerol by an Escherichia coli cardiolipin synthase. J. Biol. Chem. 291, 25144–25153.

Mason, E.A., McDaniel, E.W., 1988. Transport Properties of Ions in Gases. John Wiley & Sons, New York.

Mason, E.A., Schamp Jr, H.W., 1958. Mobility of gaseous ions in weak electric fields. Ann. Phys. (San Diego, CA, U. S.) 4, 233–270.

Mileykovskaya, E., Dowhan, W., 2000. Visualization of phospholipid domains in Escherichia coli by using the cardiolipin-specific fluorescent dye 10-N-nonyl acridine orange. J. Bacteriol. 182, 1172–1175.

Mileykovskaya, E., Dowhan, W., 2005. Role of membrane lipids in bacterial division-site selection. Curr. Opin. Microbiol. 8, 135–142.

Mileykovskaya, E., Ryan, A.C., Mo, X., Lin, C.C., Khalaf, K.I., Dowhan, W., Garrett, T.A., 2009. Phosphatidic acid and N-acylphosphatidylethanolamine form membrane domains in Escherichia coli mutant lacking cardiolipin and phosphatidylglycerol. J. Biol. Chem. 284, 2990–3000.

Miller, L.T., 1982. Single derivatization method for routine analysis of bacterial whole-cell fatty-acid methyl-esters, including hydroxy-acids. J. Clin. Microbiol. 16, 584–586.

Nishijima, M., Saeki, T., Tamori, Y., Doi, O., Nojima, S., 1978. Synthesis of acyl phosphatidylglycerol from Phosphatidylglycerol in Escherichia-coli K-12 - evidence for participation of detergent-resistant Phospholipase-a and heat-labile membrane-bound factor(S). Biochim. Biophys. Acta 528, 107–118.

Okudaira, M., Inoue, A., Shuto, A., Nakanaga, K., Kano, K., Makide, K., Saigusa, D., Tomioka, Y., Aoki, J., 2014. Separation and quantification of 2-acyl-1-lysophospholipids and 1-acyl-2-lysophospholipids in biological samples by LC–MS/MS. J. Lipid Res. 55, 2178–2192.

Oursel, D., Loutelier-Bourhis, C., Orange, N., Chevalier, S., Norris, V., Lange, C.M., 2007. Lipid composition of membranes of Escherichia coli by liquid chromatography/tandem mass spectrometry using negative electrospray ionization. Rapid Commun. Mass Spectrom. 21, 1721–1728.

Paglia, G., Angel, P., Williams, J.P., Richardson, K., Olivos, H.J., Thompson, J.W., Menikarachchi, L., Lai, S., Walsh, C., Moseley, A., Plumb, R.S., Grant, D.F., Palsson, B.O., Langridge, J., Geromanos, S., Astarita, G., 2015. Ion mobility-derived collision cross section as an additional measure for lipid fingerprinting and identification. Anal. Chem. 87, 1137–1144.

Pluckthun, A., Dennis, E.A., 1982. Acyl and phosphoryl migration in lysophospholipids: importance in phospholipid synthesis and phospholipase specificity. Biochemistry 21, 1743–1750.

Poger, D., Mark, A.E., 2015. A ring to rule them all: the effect of cyclopropane fatty acids on the fluidity of lipid bilayers. J. Phys. Chem. B 119, 5487–5495.

Rouser, G., Siakotos, A.N., Fleischer, S., 1966. Quantitative analysis of phospholipids by thin-layer chromatography and phosphorus analysis of spots. Lipids 1, 85–86.

Schmid, H.H., Schmid, P.C., Natarajan, V., 1996. The N-acylation-phosphodiesterase pathway and cell signalling. Chem. Phys. Lipids 80, 133–142.

Shibuya, I., Miyazaki, C., Ohta, A., 1985. Alteration of phospholipid-composition by combined defects in phosphatidylserine and cardiolipin synthases and physiological consequences in Escherichia-coli. J. Bacteriol. 161, 1086–1092.

Stow, S.M., Causon, T.J., Zheng, X.Y., Kurulugama, R.T., Mairinger, T., May, J.C., Rennie, E.E., Baker, E.S., Smith, R.D., McLean, J.A., Hann, S., Fjeldsted, J.C., 2017. An interlaboratory evaluation of drift tube ion mobility-mass spectrometry collision cross section measurements. Anal. Chem. 89, 9048–9055.

Tan, B.K., Bogdanov, M., Zhao, J., Dowhan, W., Raetz, C.R., Guan, Z., 2012. Discovery of a cardiolipin synthase utilizing phosphatidylethanolamine and phosphatidylglycerol as substrates. Proc. Natl. Acad. Sci. U. S. A. 109, 16504–16509.

Ulmer, C.Z., Koelmel, J.P., Ragland, J.M., Garrett, T.J., Bowden, J.A., 2017. Lipid pioneer: a comprehensive user-generated exact mass template for lipidomics. J. Am. Soc. Mass Spectrom. 28, 562–565.

Gabelica, V., Shvartsburg, A.A., Afonso, C., Barran, P., Benesch, J.L., Bleiholder, C., Bowers, M.T., Bilbao, A., Bush, M.F., Campbell, J.L., Campuzano, I.D.G., Causon, T.J., Clowers, B.H., Creaser, C., De Pauw, E., Far, J., Fernandez-Lima, F., Fjeldsted, J.C., Giles, K., Groessl, M., Hogan, C.J., Hann, S., Kim, H.I., Kurulugama, R.T., May, J.C., McLean, J.A., Pagel, K., Richardson, K., Ridgeway, M.E., Rosu, F., Sobott, F., Thalassinos, K., Valentine, S.J., Wyttenbach, T., 2018. Recommendations for reporting ion mobility mass spectrometry measurements. Mass Spectrom. Rev in press.

Wang, A.Y., Cronan, J.E., 1994. The growth phase-dependent synthesis of cyclopropane fatty-acids in Escherichia-coli is the result of an rpos(Katf)-dependent promoter plus enzyme instability. Mol. Microbiol. 11, 1009–1017.

Zheng, X., Smith, R.D., Baker, E.S., 2017. Recent advances in lipid separations and structural elucidation using mass spectrometry combined with ion mobility spectrometry, ion-molecule reactions and fragmentation approaches. Curr. Opin. Chem. Biol. 42, 111–118.

Zhou, Z.W., Tu, J., Xiong, X., Shen, X.T., Zhu, Z.J., 2017. LipidCCS: prediction of collision cross-section values for lipids with high precision to support ion mobility-mass spectrometry-based lipidomics. Anal. Chem. 89, 9559–9566.

Zhou, Z.W., Shen, X., Chen, X., Tu, J., Xiong, X., Zhu, Z.J., 2018a. LipidIMMS Analyzer: integrating multi-dimensional information to support lipid identification in ion mobility - mass spectrometry based lipidomics. Bioinformatics. https://doi.org/10.1093/bioinformatics/bty661.

Zhou, Z.W., Tu, J., Zhu, Z.J., 2018b. Advancing the large-scale CCS database for metabolomics and lipidomics at the machine-learning era. Curr. Opin. Chem. Biol. 42, 34–41.